Design and Control of Hybrid Electric Light Rail Vehicles with Open Ended Winding Machines

Davide De Simone, *Member, IEEE,* Stefania Carmeli, Salvatore D'Arco, Luigi Piegari, *Senior Member, IEEE,* Pietro Tricoli, *Senior Member, IEEE.*

Abstract Light railways are a low carbon emission form of transport, but it is often difficult to electrify tracks in central urban areas. This limitation can be avoided by integrating an on-board battery storage connected to the dc bus of the traction inverter with a boost dc/dc converter. However, the boost converter requires a bulky inductor and introduces additional power losses that are undesirable. This paper proposes to replace the standard induction motor with an open ended winding induction motor connected at one end to the overhead line with the traction inverter and to the other end to a battery with a second inverter in order to reduce the power losses of the traction drive. The paper addresses design and control aspects for light rail vehicles with open ended winding induction machines when the power supply is partly from the overhead line and partly from the on board battery. Moreover, the paper studies in detail the hybrid operations of the traction system i.e. when the overhead line charges the battery during coasting or at the stops. Finally, numerical simulations for a real use case are presented to quantify the reduction of power losses in comparison to the standard solution.

Index Terms— Open ended winding machines, Light Rail Vehicles, Hybrid Electric LRV, Zero emission transport.

I. INTRODUCTION

Light railways are a low carbon emission form of transport in comparison to conventional cars and busses but, in many cases, it is difficult to fully electrify tracks for the challenges connected to power network upgrades or for aesthetic reasons in places of cultural interest. Batteries have seen a significant development in their application to road transport over the last few years and several hybrid and electric vehicles have been recently introduced to the market. This has increased the interest in batteries also for rail applications, especially when the distance covered in battery-only mode is up to 100 km. The application of batteries is particularly suitable for light rail vehicles (LRVs), as the extension of the line without the overhead line is typically limited to a few kilometres in city centres.

The integration of batteries in the traction system of electric LRVs is challenging because the voltage of the overhead line, typically dc, may vary between −33% and +20% of the nominal value [1], while the terminal voltage of a lithium battery varies with the state of charge (SOC) between −26% to +14% of the nominal value [2]. To

address this issue, the battery pack is connected to the dc bus of the traction inverter with a boost dc/dc converter [3], [4] that compensates for the variations of both the overhead line and battery voltages. When the LRV is fed by the overhead line, the boost dc/dc converter operates in current mode by regulating the charging/discharging current of the battery; when the LRV is powered by the battery, the converter operates in voltage mode by regulating the voltage of the dc bus. The dc/dc converter also offers higher flexibility for the design of the battery pack, as the nominal voltage can be reduced by a factor of up to 2-3 compared to the nominal voltage of the overhead line. This enables the design of battery packs with lower number of cells in series but with more parallel strings, thus, increasing the availability of the system and reducing the complexity of the battery management system [5]. The main disadvantages of a dc/dc converter are the need of an additional inductor to boost the battery voltage and the need of switching at high frequency to reduce its inductance resulting in additional weight and power losses. In this configuration the energy exchanged by the battery and the motor always involves two power converters, i.e. the battery dc/dc converter and the traction voltage source inverter (VSI).

Alternatively, the battery can be directly connected to the dc-bus of the traction inverter, while the overhead line is connected through a dc/dc converter [6]. This configuration offers advantages if the overhead line has a voltage different from the dc-bus, or for LRVs travelling on sections at different voltage levels [7]. The dc/dc converter in this case is normally a buck-type and does not require additional power filters. However, the battery imposes the

Davide De Simone, Stefania Carmeli and Luigi Piegari are with the Department of Electronics, Information and Bioengineering, Politecnico di Milano, 20133 Milano, Italy (e-mail: davide.desimone@polimi.it; stefania.carmeli@polimi.it; luigi.piegari@polimi.it).

Salvatore D'Arco is with the Department Energy Systems, SINTEF Energy Research, Norway (email: salvatore.darco@sintef.no).

Pietro Tricoli is with the Department of Electronic, Electrical, and Systems Engineering, University of Birmingham, Birmingham, B15 2TT, UK (email: p.tricoli@bham.ac.uk)

dc bus voltage, leading to a lower utilisation of the traction inverter when the current is high, or the SOC is low. In this configuration the energy exchanged by the overhead line and the motor always involves two power converters, i.e. the overhead line dc/dc converter and the traction VSI.

In this paper it is proposed to use an open-ended winding induction motors (OEMs) connected to VSIs with one of them fed by the overhead line while the other fed by the battery. In this configuration the energy flows always in one power converter but when the overhead line recharges the battery. This implies an overall higher efficiency of the proposed solution. Moreover, as the two dc-links are isolated, different voltage levels can be selected to increase the number of levels of the voltage across the motor [8]. Furthermore, the absence of a common dc-link does not cause any common-mode current and does not require means to suppress it [9].

The main advantages of the OEM with two inverters over a standard traction drive configuration without batteries are the lower kVA rating of each inverter for a given power rating of the motor drive and possibilities for fault-tolerant operation [10]. The disadvantages are a higher total kVA rating of the converters and increased conduction losses. However, when considering the presence of batteries, it has not been investigated yet if the removal of the dc/dc converter compensates for the higher losses due the additional inverter and if a suitable control of the two inverters can improve regenerative braking. This paper addresses this gap in the literature. Moreover, it provides a detailed study on how the charging from the overhead line can be optimised during coasting or stopping times. More specifically, the main contributions of the paper can be summarized as following:

- Proposal of a new traction drive that eliminates the boost dc to dc converter for the battery and saves the weight and the space of the boost inductor.
- Introduction of a new collinear modulation of the two inverters to manage the energy exchange between the overhead line and the battery; in this way it is possible to the charge and discharge the battery while respecting the requirement of the LRV and the voltage and current limits of the traction drive.
- Definition of a control strategy that charges the battery only when the traction power demand is lower than the maximum allowing the line inverter to be designed for the same power as the state-of-the-art case.

Finally, this paper quantifies with numerical simulations the benefits in terms of power losses and battery sizing for an open-ended machine drive compared to standard solution with one inverter and one dc/dc converter. This is based on a case study modelled on a LRV route in Birmingham. To provide comparable results, the traditional drive with boost converter and the proposed OEM drive configurations have been tested in similar conditions, i.e the same route, battery, line inverter, and motor.

II. ELECTRICAL DRIVE CONFIGURATION AND CONTROL

As discussed in the introduction, the most common way to integrate batteries on LRVs is through a boost dc/dc converter, as shown in Fig. 1(a). In this arrangement, the biggest component is the power inductor that must be designed for the nominal dc current and with an inductance large enough to keep the current ripple within a fraction of the nominal value. In the proposed configuration, shown in Fig. 1(b), there is no need of a power inductor as the boost effect is obtained by the inductance of the open-ended motor windings. The line inverter is connected to the overhead line, while the battery inverter is connected to the battery. The following sections describe the proposed collinear modulation technique and the control strategy for the proposed OEM drive.
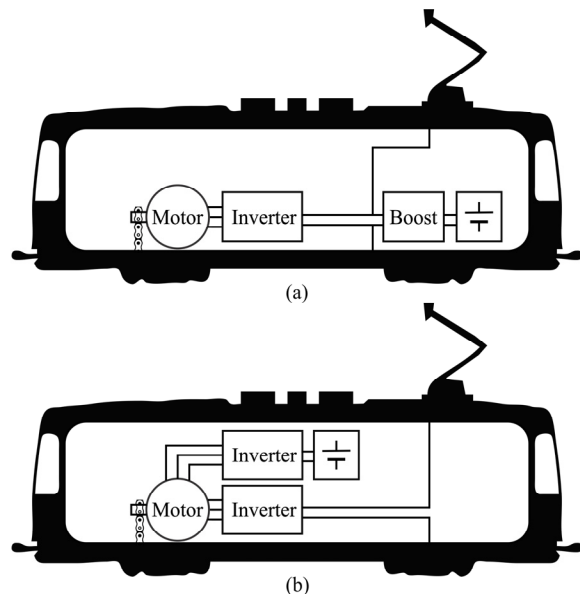

Fig. 1 Configurations to integrate batteries onboard a light electric vehicle: (a) with boost dc/dc converter.; (b) with open ended winding motor.

A. Collinear modulation

The OEM of Fig. 1(b) is fed by two voltage source inverters: connected on the dc side to the overhead line and to the battery respectively.

The motor torque and flux are controlled according to the well-known field-oriented control strategy which determines the reference stator voltage as function of the line inverter voltage and the battery inverter voltage (Fig. 2) as follow:

$$\overline{v}_m = \overline{v}_L + \overline{v}_B \tag{1}$$

where the overline indicates vector quantities while the corresponding amplitudes are indicated without the overline.

Several approaches have been proposed in scientific literature to control OEM [11]-[15]. Starting from the idea of [15], the present paper proposes a modulation strategy which regulates the power sharing between the two inverters maintaining the generated voltage space vectors in phase with the output voltage. Considering the power

balance between the line inverter power p_L, the battery power p_B and the motor power p_m:

$$p_m = p_L + p_B \qquad (2)$$

the power sharing between the two inverters can be obtained introducing the factor k defined as the ratio between the line inverter power and the motor power as shown in (3):

$$\begin{cases} p_L = kp_m \\ p_B = (1-k)p_m \end{cases}. \qquad (3)$$

Considering that the two inverters share the same current and their voltages are controlled to be aligned, from (3) it is possible to write:

$$\begin{cases} v_L = kv_m \\ v_B = (1-k)v_m \end{cases}. \qquad (4)$$

The variation range of the parameter k is related to the compliance with the maximum ratings of the power converters. Considering the relationship between the output voltages of the inverters and the reference motor voltage, for a sinusoidal PWM in linear region, the upper and lower limits of k depend on the overhead line and battery voltages respectively:

$$\begin{cases} |k|v_m = m_L \dfrac{V_{L,dc}}{2} \\ |1-k|v_m = m_B \dfrac{V_{B,dc}}{2} \end{cases} \qquad (5)$$

where m_L and m_B are the modulation indices of the line and battery inverters, $V_{L,dc}$ and $V_{B,dc}$ are the dc voltages of the overhead line and of the battery. For other modulation techniques the equations above are still valid with different coefficients.

Considering that modulation indices, m_L and m_B are lower than one, from (5) it results:

$$\begin{cases} |k|v_m \leq \dfrac{V_{L,dc}}{2} = v_{L,max} \\ |1-k|v_m \leq \dfrac{V_{B,dc}}{2} = v_{B,max} \end{cases} \qquad (6)$$

The solutions of (6) are:

$$\begin{cases} -\dfrac{v_{L,max}}{v_m} \leq k \leq \dfrac{v_{L,max}}{v_m} \\ 1 - \dfrac{v_{B,max}}{v_m} \leq k \leq 1 + \dfrac{v_{B,max}}{v_m} \end{cases} \qquad (7)$$

To comply with (7), the limit values for the sharing factor k are:

$$\begin{cases} k_{min} = \max\left(-\dfrac{v_{L,max}}{v_m} ; 1 - \dfrac{v_{B,max}}{v_m} \right) \\ k_{max} = \min\left(\dfrac{v_{L,max}}{v_m} ; 1 + \dfrac{v_{B,max}}{v_m} \right) \end{cases}. \qquad (8)$$

In addition to the sharing factor limits defined in equation (8), when the external grid is available, to prevent the battery supplying the motor, k_{min} is limited to one.
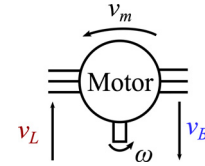

Fig. 2 Battery voltage, motor voltage, and battery voltage positive directions.

B. Regulation of the power sharing

LRVs propulsion motors voltage and current are defined by the control system with the aim of satisfying a specific speed profile request. The adoption of OEM configuration together with the collinear modulation strategy allows to reduce the weight and losses related to the power inductor of the boost dc/dc converter of traditional motor configuration, taking advantage of the motor inductance.

The different operating conditions are represented in Fig. 3. Let us consider traction mode operation, i.e. $p_m \geq 0$. In this case, if the motor speed ω is below its nominal value ω_b the corresponding motor voltage is lower than the maximum voltage, then the battery can be charged satisfying the condition $k > 1$. In this operation mode the line inverter voltage is in phase with the motor voltage while v_B is in phase opposition (Fig. 3b). As a consequence, the power supplied by the line inverter is higher than the motor power and the difference between them charges the battery. The maximum value of k must satisfy the line inverter and the battery inverter limitations defined by the first and second equation in (8) respectively. Given these voltage constraints, the maximum charging power for the battery is further limited by the motor current. This implies that for low load torques, the charging power is limited.
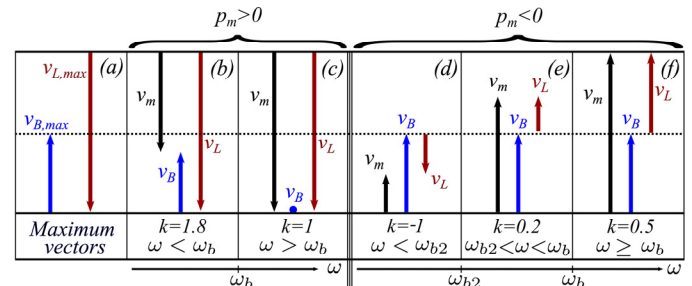

Fig. 3 Motor, line inverter, and battery inverter vector diagrams in various operating regions.

If the motor speed is greater than the nominal value (Fig. 3c), the motor voltage is equal to the maximum voltage of the line inverter (Fig. 3a) consequently the sharing factor k is limited to 1, according with the second of (8). In this case, it is not possible to charge the battery.

During braking operation mode, the motor power is negative. In this case two operating conditions should be analysed depending on the motor speed. If the motor speed is lower than a specific value, (ω_{b2} in Fig. 3d), the motor voltage is lower than the maximum battery inverter voltage and the battery is charged by both the regenerative braking and the power drawn by the contact line. In this case, the sharing factor k is lower than zero making the line inverter

voltage and the battery inverter voltage in phase opposition. If the motor speed is between ω_{b2} and ω_b (Fig. 3e) the maximum battery inverter voltage is lower than the motor voltage and, consequently the line inverter voltage must be in phase with the battery inverter voltage. In this condition, achieved by keeping k higher than zero but lower than one, a fraction of the regenerative power is injected into the contact line. Finally, if the motor speed is greater than the nominal value (Fig. 3f), the sharing factor is set to keep the battery inverter voltage to the maximum and to reach the motor nominal voltage with the line inverter.

Without overhead line, the line inverter is bypassed, the power sharing algorithm is ignored, and the battery inverter is controlled as a normal traction drive. It is worth noting that in the areas without overhead line, the maximum voltage that can be applied to the motor is limited by the battery voltage. If the battery inverter cannot generate the nominal motor voltage, it will be necessary to reduce the machine flux linkage also when running below its nominal speed.

III. System design considerations

In this section, the proposed OEM drive is compared with the standard drive in terms of design of the power converters.

A. Boost dc/dc converter design

The components of the dc/dc converter are designed according to the voltage of the overhead line and the maximum battery current. The maximum battery current can be calculated considering the minimum battery voltage:

$$I_B = \frac{P_{boost}}{N_B \cdot V_{B,dc,\min}} \tag{9}$$

where N_B is the number of series battery modules. The boost inductance is related to the maximum current ripple:

$$L = \frac{V_{L,dc}}{4\Delta I f_{sw}} \tag{10}$$

where ΔI is the maximum current ripple and fsw is the switching frequency. Moreover, the RMS current depends on the current ripple ΔI according to:

$$I_{rms} = \sqrt{I_{B,dc}^2 + \frac{\Delta I^2}{3}} \tag{11}$$

The additional losses due to current ripple have a more relevant effect on the system efficiency during low power operation. Fig. 4 shows the boost converter efficiency for different output powers and different values of the current ripple. As visible from the figure, the reduction of system efficiency due to current ripple is more significant with low loads.

B. Drive inverter design

According to the configuration shown in Fig. 1, the main drive inverter is connected directly to the overhead line. Its semiconductor devices must be designed considering the maximum voltage on the line, including transient over voltages, and the motor maximum current.

C. Design of the inverters of the OEM

Since in the proposed powertrain the motor windings are open-ended, the rated motor current must be used for the design of both the line and the battery inverters. The semiconductors devices must be chosen based on the line voltage for the line inverter, and the maximum battery voltage for the battery-side inverter. As the battery is used only when the LRV travels at low speed, the battery inverter can be designed with a lower blocking voltage than the line inverter, substantially reducing switching losses.

D. Design of the battery

The design of the battery is the same for both cases. Given the system power rating and maximum distance travelled by the light railway vehicle in battery-only mode, the battery can be designed following an energy approach or a power approach. Both strategies start by estimating the vehicle total energy needs, E_0, and power profiles when the light rail vehicle travels without the overhead line.
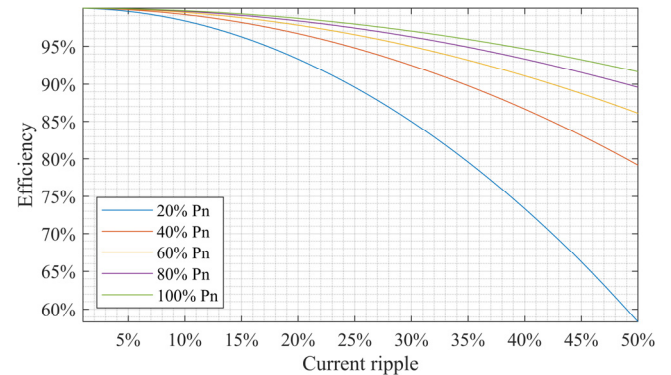

Fig. 4 Boost dc/dc converter efficiency drop as a function of output power and sizing current ripple.

Batteries are not normally used up to their full capacity to increase the lifetime, so the state of charge is limited between a minimum and a maximum value, namely $SoC_{\min}$ and $SoC_{\max}$. By introducing the utilization range γ:

$$\gamma = SoC_{max} - SoC_{min} \tag{12}$$

the battery energy can be approximated dividing E_0 by γ. The power limitations of the batteries are related to thermal effects, so manufacturers commonly provide the maximum charging and discharging C-rates, which are defined as the ratio between maximum battery current and rated capacity in Ah.

To meet the off-grid energy requirement of the LRV, as well as to accommodate the maximum expected charging and discharging powers, the battery needs to have a capacity greater than the required energy and a C-rate sufficient to satisfy the power requirements of the LRV. In consideration of the concerns surrounding reliability and lifespan in public transportation, the design of the battery for the LRV can also be approached in terms of rated power. This alternative approach aims to alleviate the potential issues arising from a stringent sizing C-rate, which may not be suitable for applications where reliability and

lifespan are of utmost importance [16]. By following this approach, the target maximum charging and discharging C-rates, C_{ch} and C_{dch}, are first selected. The battery capacity in Ah is calculated as:

$$\begin{cases} Ah_{ch} = A_{ch} / C_{ch} \\ Ah_{dch} = A_{dch} / C_{dch} \\ Ah = \max(Ah_{ch}, Ah_{dch}) \end{cases} \quad (13)$$

where A_{ch} and A_{dch} represent the required current in charge and discharge operation. The battery capacity in Ah is, then, converted into the corresponding battery energy in kWh to check if the utilization range (12) is acceptable. If this condition is not met, the battery capacity is increased until the utilization range reaches the desired value.

IV. CASE STUDY DEFINITION

This section introduces the case study for the comparison of the two traction systems.

A. Reference route

The two systems have been tested on a line having similar characteristics to the LRV line between Wolverhampton St George and Edgbaston Village in Birmingham (UK) and on a smaller section of the same route between Bull Street and Edgbaston Village.

The LRV line was extracted using *gpx studio* [17] from the map by measuring the road distance of the railway between the stops of the corresponding line, and storing the extracted data in a lookup table. The speed and distance profiles have been built using the published timetable and the public data available on the LRV used for this line. As shown in Fig. 5, the LRVs travel in a suburban area at a maximum speed of approximately 70 km/h, and in an urban area where the maximum speed is limited to 40 km/h. The low-speed region is located within the city-center of Birmingham, where the overhead line is not present. The LRV calls at predefined stops and waits for approximately 30 s to allow passengers to alight.

B. Vehicle under test

The LRV under analysis (Urbos 3) has a tare mass of 56,000 kg and a passenger capacity of 210, for a total mass of 72,800 kg at full load. The powertrain is divided in 12 traction induction motors, equally distributed across the cars [18]. The main specifications of the traction motors are summarized in Table 1.

C. Battery design

The battery is designed in this paper with a voltage equal to half the nominal voltage of the overhead line. To achieve this requirement, 101 lithium polymer cells model 8773160K are connected in series. The voltage limits for the battery pack are reported in Table 2. A maximum charging C-rate of 3 and a discharging C-rate of 10 have been selected as a good trade-off between performance and lifetime.

The discharging and charging power profiles of the sections of the line without overhead line have been

calculated and have shown that, according to the selected C-rates, the most stringent condition is related to decelerations in the urban area. The charging peak power has been thus selected to design the battery, eventually resulting in an energy of 12.3 kWh.

Moreover, the maximum state of charge for the battery was limited to 70% to reduce calendar ageing [19],[20].
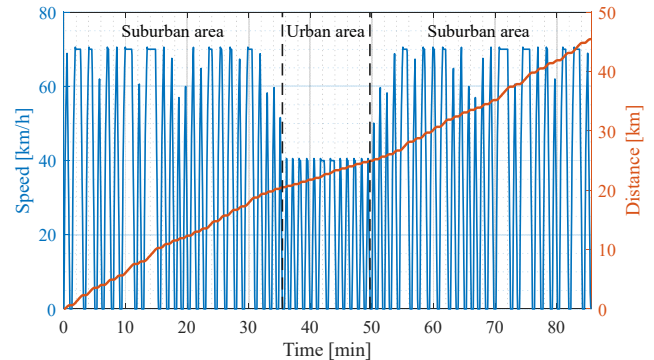

Fig. 5 Blue line: LRV speed profile over time. Orange line: LRV position over time.

TABLE 1
MOTOR PARAMETERS

Parameter	Value
Nominal power	80 kW
Nominal apparent power	99 kVA
Nominal voltage	460 V
Nominal current	124 A
Nominal frequency	50 Hz
Nominal power factor	0.88
Nominal efficiency	0.92
Number of poles	2

TABLE 2
BATTERY DATA

Parameter	Value
Nominal voltage	373.7 V
Maximum voltage	423.7 V
Minimum voltage	277.7 V
Battery size	12.3 kWh

D. Main inverter design

Most of the line is supplied with a 750V overhead line. Given the variation of the actual voltage and the presence of parasitic inductances, the voltage rating of the semiconductor devices has been chosen at 1,700V. The current rating of the semiconductors has been set on the peak value of the rated current in Table 1 plus a safety margin. Three *CM200DY-34T* 1,700V half bridges from Mitsubishi Electric [21] have been selected for the line inverter and a switching frequency of 10 kHz has been chosen. In Table 3 the main characteristics of the line inverter semiconductors are summarized. Some of the data in the table were presented as numerical values in the datasheet, while others, such as the collector-emitter saturation voltage at no load, IGBT conduction resistance, diode forward voltage at no load, and the diode conduction resistance, were obtained from the diagrams reported in the datasheet. The same process was repeated for all the component's data tables in the following paragraphs.

E. Boost dc/dc converter design

Given the motor rated power, the boost dc/dc converter rating is set at 40 kW, as the speed of the LRV in the urban area is less than 40 km/h. Using the minimum battery voltage of Table 2, the maximum battery current at nominal power is 132 A. According to this value and the maximum voltage of the overhead line, *CM150DX-34SA* half bridge semiconductor devices [22] have been chosen. Their main specifications are summarized in Table 4. The inductor has been designed to maintain an efficiency between 90% and 95% at the minimum power output of 20% of the rated value. According to this requirement, the current ripple should be within the range [17%, 24%], leading to the selection of a current ripple of 20% for the design of the half bridge converter inductance. Considering a switching frequency of 20 kHz, by applying equation (10) the boost converter inductor has an inductance of 401 μH.

TABLE 3

CM200DY-34T IGBT HALF BRIDGE MAIN DATA

Parameter	Value
Maximum collector-emitter voltage	1700 V
Collector current	200 A
Collector-emitter saturation voltage	0.8 V
Conduction resistance	5 mW
Turn-on energy loss	56.3 mJ
Turn-off energy loss	52.4 mJ
Reverse recovery energy	22.7 mJ
Diode forward voltage	1.25 V
Diode conduction resistance	6.4 mW

TABLE 4

CM150DX-34SA BOOST DC/DC IGBT DATA

Parameter	Value
Maximum collector-emitter voltage	1700 V
Collector current	150 A
Collector-emitter saturation voltage	1 V
Conduction resistance	5.4 mW
Turn-on energy loss	26 mJ
Turn-off energy loss	46 mJ
Reverse recovery energy	32 mJ
Diode forward voltage	1 V
Diode conduction resistance	14mW

F. OEM inverter design

For the OEM, the voltage rating for the battery inverter has been set accordingly to the maximum battery voltage in Table 2. A set of three 650V half bridges from Mitsubishi Electric *CM200DY-13T* [23] was chosen. Their main specifications are summarized in the Table 5.

G. G. Boost dc/dc converter powertrain control

In the traditional configuration of Fig. 1 (a), the traction is controlled by the energy management system (EMS). When driving in the city center in the absence of overhead line ($LA = 0$), a lower driving speed is required. In this scenario, the EMS controls the boost dc/dc converter to supply the traction drive. Outside the urban areas, the LRV is fed by the overhead line ($LA = 1$) and the EMS controls the boost dc/dc converter to charge the battery up to a *SoC** of 70%. During this process, the EMS ensures that the light rail vehicle draws no more than its rated power not to overload the external line. This is done by limiting the

charging rate of the battery accordingly to the power drawn from the motor. The maximum charging power is then selected to be compliant with the maximum charging C-rate. As the battery SoC approaches the reference value, the boost dc/dc converter enters stand-by mode. A block diagram of the control system is given in Fig. 6.

H. OEM powertrain control

The energy management in the OEM powertrain is undertaken by the controller of Fig. 7. When driving in the city center ($LA = 0$), the voltage reference for the line inverter is set to zero and the converter enters stand-by mode, the motor voltage vector is generated by the battery inverter.

When the vehicle exits the urban area ($LA = 1$) and the battery must be charged, the line inverter voltage is divided between the motor and the battery inverter. The SoC regulator generates a battery power reference based on the SoC error. This value is then saturated dynamically between the maximum battery power and the power difference between the nominal power of the LRV and the motor power. The saturated battery power reference p_B* is then converted into the sharing factor k with equation (3). The resulting sharing factor is then saturated to satisfy the voltage limits of the converters using equations (8).
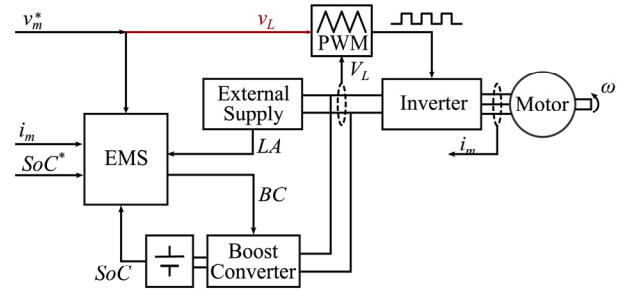

Fig. 6 Logic diagram of boost dc/dc converter control.

TABLE 5

CM200DY-13T IGBT HALF BRIDGE MAIN DATA

Parameter	Value
Maximum collector-emitter voltage	650 V
Collector current	200 A
Collector-emitter saturation voltage	0.75 V
Conduction resistance	2.5 mW
Turn-on energy loss	3.1 mJ
Turn-off energy loss	10.8 mJ
Reverse recovery energy	4.6 mJ
Diode forward voltage	0.5 V
Diode conduction resistance	5.5 mW

V. NUMERICAL RESULTS

The two powertrains were tested using the speed profile defined in section IV in the complete (from Wolverhampton St George to Edgbaston Village) and reduced (from Bull Street to Edgbaston Village) variants by means of simulations. The results for the complete and reduced driving paths are illustrated in Fig. 8 and Fig. 9, respectively. The top part of the first plot shows the distance traveled, highlighting the urban and suburban

areas, while the bottom part shows the battery SoC profiles for the two strategies. In the second plot urban and suburban areas are delimited by vertical lines. In the complete driving path, the two systems start with a SoC of 70%, and for the initial 36 minutes of travel in the suburban region, the battery converters are both in standby mode. As the vehicle enters the urban area the battery is activated to supply the traction motors. In the traditional powertrain, the boost converter raises the battery voltage to match the nominal voltage of the system's dc bus, which is 750 V, and feeds the main inverter.

In the OEM powertrain, the motor is powered only by the inverter connected to the battery, which reduces the number of power conversion stages. However, the voltage of the dc bus on the battery inverter of the OEM powertrain is not sufficient to supply the motor up to its nominal voltage. As a result, the motor needs to be operated in the field weakening region at approximately half of its nominal speed, resulting in increased losses of the motor during the acceleration phases.

To illustrate this phenomenon, Fig. 10 displays the power loss of the motor in both powertrains. During acceleration, the drive demands high torque from the motor. In the OEM drive, operating in the reduced flux region leads to increased motor losses when high torque is required, although it improves efficiency when the motor runs at a constant speed. In both powertrains, when the tram comes to a stop, the motor flux is reduced to minimize system losses. When the LRV needs to start again, the motor flux is restored, resulting in loss spikes that are evident before and after each stop for both configurations.

The figures show that the OEM powertrain has higher efficiency in the urban region, leading to 14% less discharge of the battery, as shown by the Battery Energy column of
Table 6.

When the tram returns into the suburban region, the battery is recharged to its initial SoC. While the OEM powertrain demonstrates greater efficiency in the urban area, the charging power for the battery is heavily influenced by external factors such as the required motor speed and torque.
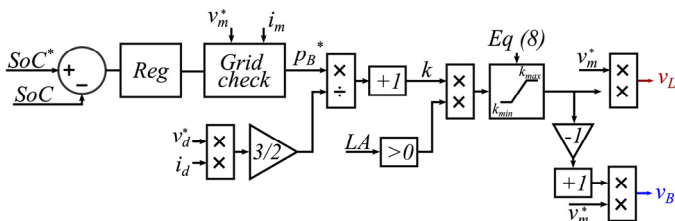

Fig. 7 OEM energy management system schematic.

These constraints reduce the average charging power, resulting in longer recharging times and increased overall losses. The trade-off between the higher efficiency in the urban region and the lower efficiency during the charging process contributes to an overall 1% reduction in the consumption of the OEM powertrain compared to the

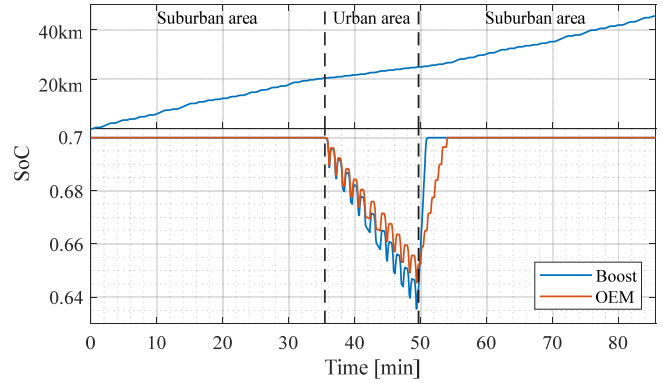standard powertrain in the case the complete driving path.

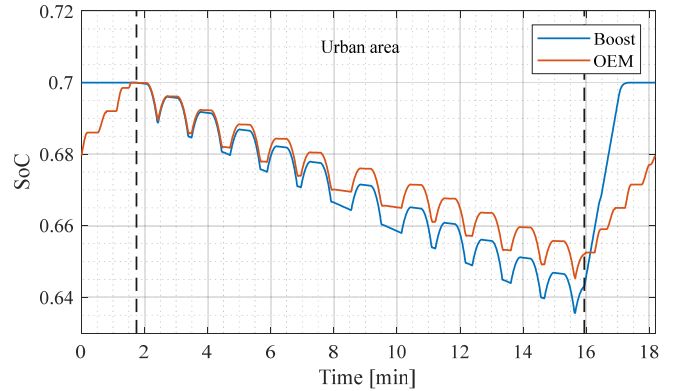Fig. 8 Battery state of charge over time with complete driving path.

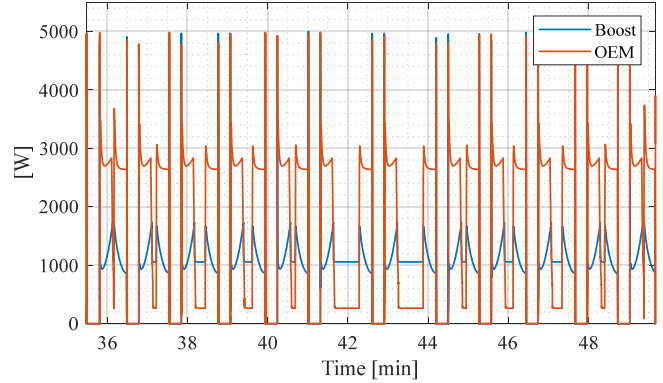Fig. 9 Battery state of charge over time with reduced driving path.

Fig. 10 Motor losses as a function of time, focus on the urban area.

TABLE 6
SUMMARY RESULTS OF COMPLETE PATH AND REDUCED PATH

Type	Total Path	Reduced Path	Urban	Battery Energy
Standard	1.34 kWh/km	1.62 kWh/km	1.66 kWh/km	616 Wh
OEM	1.33 kWh/km	1.56 kWh/km	1.42 kWh/km	527 Wh
Relative difference	−1%	-4%	-14%	−14%

If the shorter driving path including more off-grid areas is considered, the overall energy for doing a round trip is 4% lower for the OEM powertrain compared to the standard powertrain. This is due to the fact that once the charging phase is completed, the two systems have the same efficiency, thus, reducing the relative path supplied by the overhead line amplifies the efficiency difference.

VI. CONCLUSIONS

In this paper a new power architecture to integrate batteries on hybrid LRV traction drives has been proposed. The traditional power converter topology to integrate batteries on LRV is based on a bidirectional boost-converter interfacing the battery on the dc-bus of the vehicle in parallel with the line supply and a two-level inverter to supply the traction motor. The bidirectional boost converter presents a large and heavy inductor that must be installed onboard.

The proposed power architecture is based on the use of an OEM: one side of the motor windings is supplied by means of the traditional inverter connected to the line; the other side of the motor windings is supplied by another two-level inverter connected to the battery. In this way, the large inductor is removed and there is no need to push energy from the lower voltage of the battery to the higher voltage of the dc-bus. Indeed, the traction motor is supplied at lower voltage when working in battery mode. This limits the speed of the LRV in battery mode. However, this is not an issue since battery mode is used in the urban centers where the speed is, therefore, limited.

The effectiveness of the proposed solution has been assessed by comparing it with the traditional power system (i.e. the one with the boost converter). Both systems have been simulated for a real route in the city of Birmingham (UK) where the suburban region is supplied with an overhead line while the urban section is not electrified. Two scenarios have been simulated: one with a long suburban path and another with a shorter suburban part. The simulations have shown that the OEM drive has higher efficiency for all the scenarios. In particular, for the first case (i.e. longer suburban path) the energy consumption is reduced by 1% while for the second case (i.e. shorter suburban path) the energy saving is 4%. It is worth noting that, for battery-only operations, the proposed solution achieves a reduction of 14% of energy consumption. The considerably higher efficiency of the proposed drive in battery-only mode implies a lower use of the battery itself and its consequent longer lifetime, reducing the overall cost of the system. Alternatively, a smaller battery could be used, saving weight and installation cost.

The OEM drive has shown a relatively longer battery recharge time related to its limitations in terms of power sharing between the overhead line and the battery. The possibility of having an external charger at the terminal stations could furtherly increase the advantages of the proposed solution. This aspect will be investigated in future research.

VII. REFERENCES

[1] H. J. Kaleybar, M. Brenna, F. Foiadelli, S. S. Fazel, and D. Zaninelli, 'Power Quality Phenomena in Electric Railway Power Supply Systems: An Exhaustive Framework and Classification', *Energies*, vol. 13, no. 24, p. 6662, Dec. 2020, doi: 10.3390/en13246662.

[2] S. Barcellona, L. Codecasa, S. Colnago, and L. Piegari, 'Cycle Aging Effect on the Open Circuit Voltage of Lithium-Ion Battery', in *2023 IEEE International Conference on Electrical Systems for Aircraft, Railway, Ship Propulsion and Road Vehicles & International Transportation Electrification Conference (ESARS-ITEC)*, Venice, Italy: IEEE, Mar. 2023, pp. 1–6. doi: 10.1109/ESARS-ITEC57127.2023.10114896.

[3] P. Pescetto, A. Sierra-Gonzalez, F. Alvarez-Gonzalez, H. Kapeller, E. Trancho, and G. Pellegrino, 'Active Control of Variable DC-Link for Maximum Efficiency of Traction Motor Drives', *IEEE Trans. Ind. Appl.*, pp. 1–10, 2023, doi: 10.1109/TIA.2023.3267770.

[4] 'BDC546 – BRUSA'. https://www.brusa.biz/portfolio/bdc546/ (accessed Jul. 06, 2023).

[5] L. Chang, C. Ma, C. Zhang, B. Duan, N. Cui, and C. Li, 'Correlations of lithium-ion battery parameter variations and connected configurations on pack statistics', *Appl. Energy*, vol. 329, p. 120275, Jan. 2023, doi: 10.1016/j.apenergy.2022.120275.

[6] J. Xiang, J. Xu, H. Wang, C. Li, G. Cui, and Y. Peng, 'Reconfigurable Line-Side Converter for DC Voltage Matching and Ripple Suppression in Multisystem Locomotives', *IEEE Trans. Power Electron.*, vol. 36, no. 5, pp. 5832–5844, May 2021, doi: 10.1109/TPEL.2020.3026682.

[7] M. M. Bakran, H.-G. Eckel, P. Eckert, H. Gambach, and U. Wenkemann, 'Comparison of multisystem traction converters for high-power locomotives', in *2004 IEEE 35th Annual Power Electronics Specialists Conference (IEEE Cat. No.04CH37551)*, Aachen, Germany: IEEE, 2004, pp. 697–703. doi: 10.1109/PESC.2004.1355833.

[8] S. Foti, A. Testa, S. De Caro, T. Scimone, G. Scelba, and G. Scarcella, 'Multi-Level Open End Windings Multi-Motor Drives', *Energies*, vol. 12, no. 5, p. 861, Mar. 2019, doi: 10.3390/en12050861.

[9] W. Hu, C. Ruan, H. Nian, and D. Sun, 'Zero-Sequence Current Suppression Strategy With Common-Mode Voltage Control for Open-End Winding PMSM Drives With Common DC Bus', *IEEE Trans. Ind. Electron.*, vol. 68, no. 6, pp. 4691–4702, Jun. 2021, doi: 10.1109/TIE.2020.2988221.

[10] F. Meinguet, N.-K. Nguyen, P. Sandulescu, X. Kestelyn, and E. Semail, 'Fault-tolerant operation of an open-end winding five-phase PMSM drive with inverter faults', in *IECON 2013 - 39th Annual Conference of the IEEE Industrial Electronics Society*, Vienna, Austria: IEEE, Nov. 2013, pp. 5191–5196. doi: 10.1109/IECON.2013.6699978.

[11] G. Nadh, N. S. Durga, and R. S. Arun, 'Hybrid Space Vector Modulation Scheme for Dual Inverter Fed Open End Winding Induction Motor Drive for Improved Harmonic Distortion', in *2018 8th IEEE India International Conference on Power Electronics (IICPE)*, JAIPUR, India: IEEE, Dec. 2018, pp. 1–6. doi: 10.1109/IICPE.2018.8709455.

[12] A. Somani, R. K. Gupta, K. K. Mohapatra, K. Basu, and N. Mohan, 'Modulation strategies for direct-link drive for open-end winding AC machines', in *2009 IEEE International Electric Machines and Drives Conference*, Miami, FL, USA: IEEE, May 2009, pp. 1863–1868. doi: 10.1109/IEMDC.2009.5075457.

[13] I. J. Smith and J. Salmon, 'High-Efficiency Operation of an Open-Ended Winding Induction Motor Using Constant Power Factor Control', *IEEE Trans. Power Electron.*, vol. 33, no. 12, pp. 10663–10672, Dec. 2018, doi: 10.1109/TPEL.2018.2806740.

[14] Y.-F. Jia *et al.*, 'Control Strategy for an Open-End Winding Induction Motor Drive System for Dual-Power Electric Vehicles', *IEEE Access*, vol. 8, pp. 8844–8860, 2020, doi: 10.1109/ACCESS.2020.2964105.

[15] Y.-F. Jia, L. Chu, N. Xu, Y.-K. Li, D. Zhao, and X. Tang, 'Power Sharing and Voltage Vector Distribution Model of a Dual Inverter Open-End Winding Motor Drive System for Electric Vehicles', *Appl. Sci.*, vol. 8, no. 2, p. 254, Feb. 2018, doi: 10.3390/app8020254.

[16] B. Chen, B. Cai, W. Shangguan, and J. Wang, 'Data-Driven Failure Characteristics and Reliability Analysis for Train Control On-Board Subsystem', *IEEE Access*, vol. 7, pp. 126489–126499, 2019, doi: 10.1109/ACCESS.2019.2938851.

[17] 'gpx.studio — the online GPX file editor'. https://gpx.studio/ (accessed Jul. 06, 2023).

[18] 'West Midlands Metro rolling stock', *Wikipedia*. Jul. 02, 2023. Accessed: Jul. 06, 2023. [Online]. Available: https://en.wikipedia.org/w/index.php?title=West_Midlands_Metro_rolling_stock&oldid=1162978093

[19] W. Vermeer, G. R. Chandra Mouli, and P. Bauer, 'A Comprehensive Review on the Characteristics and Modeling of Lithium-Ion Battery

Aging', *IEEE Trans. Transp. Electrification*, vol. 8, no. 2, pp. 2205–2232, Jun. 2022, doi: 10.1109/TTE.2021.3138357.

[20] E. Prada, D. Di Domenico, Y. Creff, J. Bernard, V. Sauvant-Moynot, and F. Huet, 'Physics-based modelling of LiFePO4-graphite Li-ion batteries for power and capacity fade predictions: Application to calendar aging of PHEV and EV', in *2012 IEEE Vehicle Power and Propulsion Conference*, Oct. 2012, pp. 301–308. doi: 10.1109/VPPC.2012.6422717.

[21] 'cm200dy-34t_e.pdf'. Accessed: Jul. 06, 2023. [Online]. Available: https://www.mitsubishielectric.com/semiconductors/content/product/powermodule/igbt/t_series/cm200dy-34t_e.pdf

[22] 'cm150dx-34sa_e.pdf'. Accessed: Jul. 06, 2023. [Online]. Available: https://www.mitsubishielectric.com/semiconductors/content/product/powermodule/igbt/s_series/cm150dx-34sa_e.pdf

[23] 'cm200dy-13t_e.pdf'. Accessed: Jul. 06, 2023. [Online]. Available: https://www.mitsubishielectric.com/semiconductors/content/product/powermodule/igbt/t_series/cm200dy-13t_e.pdf